

Experimental investigation of heat generation during the mixing of granular materials in an overhead stirrer

Francisco Kisuka¹, Rafael Rangel², Colin Hare³, Vincenzino Vivacqua⁴, and Charley Wu¹

¹University of Surrey

²International Center for Numerical Methods in Engineering

³Newcastle University

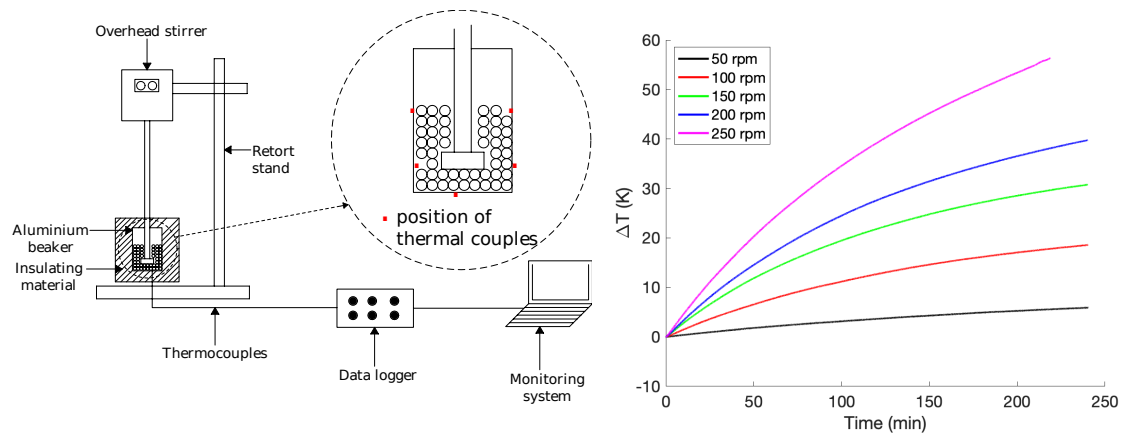
⁴UCB Pharma SA Belgium

March 26, 2023

Abstract

Bladed mixers are widely used for processing granular materials where significant mechanical energy is required to produce the desired blend. Some mechanical energy is dissipated within the granular medium, generating heat during this process. However, our knowledge of the heat generation mechanisms without external thermal loads is still lacking. This study uses an overhead stirrer to mix granular materials and investigate heat generation by monitoring the temperature changes in the granular bed. Additionally, first-order kinetic equations are used to extrapolate the experimental data to a thermal equilibrium where the heat generation and heat loss rates are equal. Lead, steel, and glass particles are used under various operating conditions. It is observed that metallic particles heat up faster owing to their lower heat capacity. Also, increasing the rotation speed, fill ratio and particle size result in a greater temperature increase. Moreover, flat blades induce more heat generation compared to tilted blades.

Graphical Abstract



Experimental investigation of heat generation during the mixing of granular materials in an overhead stirrer

Francisco Kisuka^a, Rafael L. Rangel^b, Colin Hare^{a,c}, Vincenzino Vivacqua^d and Chuan-Yu Wu^{a,*}

^a*School of Chemistry and Chemical Engineering, University of Surrey, Guildford GU2 7XH, United Kingdom*

^b*International Centre for Numerical Methods in Engineering (CIMNE), Universitat Politècnica de Catalunya, 08034 Barcelona, Spain*

^c*School of Engineering, Newcastle University, Newcastle upon Tyne NE1 7RU, United Kingdom*

^d*Johnson Matthey Technology Centre, Billingham TS23 1LB, United Kingdom*

ARTICLE INFO

Keywords:

granular mixing
heat generation
bladed mixer
overhead stirrer
temperature rise

Abstract

Bladed mixers are widely used for processing granular materials where significant mechanical energy is required to produce the desired blend. Some mechanical energy is dissipated within the granular medium, generating heat during this process. However, our knowledge of the heat generation mechanisms without external thermal loads is still lacking. This study uses an overhead stirrer to mix granular materials and investigate heat generation by monitoring the temperature changes in the granular bed. Additionally, first-order kinetic equations are used to extrapolate the experimental data to a thermal equilibrium where the heat generation and heat loss rates are equal. Lead, steel, and glass particles are used under various operating conditions. It is observed that metallic particles heat up faster owing to their lower heat capacity. Also, increasing the rotation speed, fill ratio and particle size result in a greater temperature increase. Moreover, flat blades induce more heat generation compared to tilted blades.

1. Introduction

Granular mixing is a unit operation used widely in industrial applications such as drying, blending, agglomeration and granulation. The mixing process involves energy dissipation mainly through particle friction and plastic deformation. Consequently, some of the dissipated energy is converted into heat. The generated heat can cause a sharp and sudden increase in temperature and affect the material quality and the equipment performance, particularly for heat-sensitive materials [1–3]. For example, in pharmaceuticals, the drying process requires a controlled temperature to maintain the chemical stability of the Active Pharmaceutical Ingredients (APIs). Higher temperatures can increase the solubility of the API in any remaining solvents and cause a partial dissolution leading to agglomeration [4]. On the other hand, drying higher volumes of API requires higher temperatures to avoid bottle-necking the processing chain [5, 6]. It is, therefore, crucial to understand the heat generation mechanisms involved in applications requiring temperature control to maintain product quality.

Mixers commonly used in industrial applications include bladed mixers [7, 8], rotating drums [9, 10], agitated filter beds [11, 12], and fluidised beds [13, 14]. However, bladed mixers (e.g., the overhead stirrers) possess the advantage of their simpler design and relatively shorter blending time [15]. Moreover, such mixers are extensively used in applications that require high input power, e.g., in blending solid pellets to melt and mix the polymer [7] and their blending performance was examined by many researchers [7, 8, 16–18]. However, these studies focused mainly on the impeller torque and power consumption [7, 8], flow behaviour [16, 17], and heat transfer [18]. Little attention was paid to the energy dissipation and thermal response of the granular bed.

Understanding the flow behaviour of the granular material is crucial for establishing fundamental relations such as stress distribution and work done per unit mass during mixing. Generally, the flow behaviour is classified into three regimes based on the inertia number, I_0 , which is a function of shear rate, $\dot{\gamma}$, particle diameter, ϕ , pressure, P , and particle density, ρ (see Eq. 1).

*Corresponding author

 c.y.wu@surrey.ac.uk (C. Wu)

ORCID(s):

$$I_0 = \frac{\gamma\phi}{\sqrt{P/\rho}} \quad (1)$$

47 These are i) the slow or friction regime at $I_0 < 10^{-3}$ characterised by slow shear rates and dominant frictional forces; ii)
 48 the rapid regime at $I_0 > 10^{-1}$ dominated by inertia forces and short collisions; and iii) the intermediate regime that lies
 49 between the two, showing a more fluid-like behaviour [19–21]. Moreover, many experimental and theoretical works
 50 were dedicated to exploring the underlying mechanisms for each flow regime [22–25]. Previous experimental studies
 51 employed optical image analysis to extract two-dimensional information on particle movement during mixing [26, 27].
 52 In addition, three-dimensional information on the flow behaviour of the whole granular bed was also assessed using
 53 such techniques as positron emission particle tracking (PEPT) [28, 29], radioactive particle tracking (RPT) [30], and
 54 X-ray stereography [31, 32]. A broad review of different techniques for tracking particle dynamics during mixing was
 55 reported in Nadeem et al. [33]. Nonetheless, using numerical tools, particularly the discrete element method (DEM),
 56 enhanced our understanding of granular flow behaviour in bladed mixers [34–36].

57 During mixing, some energy is dissipated to the granular matter, and the amount of the dissipated energy is reflected
 58 through the impeller torque and system power consumption. Many studies investigated the influence of the operating
 59 conditions on the impeller torque. Experimental studies by Knight et al. [7] and Bookanokwong et al. [8] revealed that
 60 the impeller torque increases with fill ratio, particle size and blade rotational speed. Similar observations were made
 61 using DEM, indicating a clear correlation between the impeller torque and the fill ratio [11, 37]. Additionally, it was
 62 inferred that the impeller torque is significantly affected by the blade configurations, i.e., angle, size, shape and number
 63 of blades [8, 38]. Besides monitoring the impeller torque, power consumption can also be measured to examine the
 64 energy spent agitating the solid particulate medium. Bookanokwong et al. [8] performed experiments and measured
 65 the influence of material type, impeller configuration and operating conditions on the system power consumption.
 66 Despite the difficulty in accurately measuring the power, it was shown that the power consumption trends correspond
 67 to those of the impeller torque. Similarly, Gijón-Arreortúa [39] established a relationship between power consumption
 68 and a dimensionless number consisting of powder physical properties, operating conditions and blade configurations
 69 for mixing in a helical double-ribbon impeller. Recently, Bao [40] used the concept of *apparent viscosity* of granular
 70 medium and proposed a model for estimating the shaft power consumption under various agitation speeds, blade types
 71 and fill ratios.

72 Monitoring the temperature of the granular bed gives a direct reflection of not only the work done to agitate
 73 the system but also the fraction of the dissipated energy that is converted into heat. Wagner et al. [41] performed
 74 experiments on the Bohle granulator to quantify heat generation during lactose blending. An energy balance equation
 75 was developed based uniquely on the temperature of the powder and the heat loss to the surrounding. However, the
 76 energy balance equation could not account for other forms of energy, such as the kinetic energy of the powder particles,
 77 resulting in the under-prediction of power input to the system, especially at high blending speeds. Similarly, Sun
 78 et al. [42] used a horizontal-bladed mixer and examined the heat generation for the wet and dry granular matter. It
 79 was concluded that the heat generation comes mainly from plastic deformation, followed by sliding friction, and an
 80 insignificant contribution from rolling friction. Despite the interesting results, the horizontal-bladed mixer used does
 81 not represent the same flow behaviour as the vertical mixers commonly used.

82 Despite valuable insights into bladed mixers, the link between operating parameters and the thermal response of
 83 granular media is not explored in-depth. Few studies examined the influence of operating parameters on the drying
 84 process for bladed mixers with heating jackets [18, 43]. However, such studies were only limited to the heat transfer
 85 phenomenon in the presence of external heat sources, ignoring the heat generation induced by energy dissipation. This
 86 work will address the problem of heat generation without external heat sources by quantifying the temperature changes
 87 within the granular bed during the mixing process under various operating conditions for different materials.

88 2. Materials and methods

89 2.1. Experimental setup

90 The experimental setup (Fig. 1) comprises two main systems: the mixing and data acquisition systems. The mixing
 91 system is an overhead stirrer (*SciQuip Ltd, Shropshire, United Kingdom*). The overhead stirrer is connected to a power
 92 source and has a motor that can rotate at a controlled speed. The motor is mounted with an impeller which rests in
 93 a beaker containing the particles to be agitated. The impeller shaft is centrally aligned to ensure a uniform lateral

94 clearance between the internal wall of the beaker and the blade's tip. The bottom clearance between the blade and
 95 the beaker is kept constant at 10 mm. The beaker has an internal diameter of 85 mm, a height of 100 mm and a wall
 96 thickness of 1 mm. It is made of aluminium, to allow quick and uniform conduction of the generated heat. The data
 97 acquisition system comprises thermal couples, a data logger and a computer. Five thermocouples (Type K) are used
 98 to monitor the temperature changes; four are attached to the lateral wall inside and outside the beaker, and one is at the
 99 bottom outside. While attached to the thermocouples, the beaker is wrapped with adhesive aluminium tape and cotton
 100 wool to minimise direct heat exchange between the beaker and the surroundings. The thermocouples are connected
 101 to a data logger calibrated following the UKAS standard to an error of $\pm 0.5^\circ\text{C}$. The data logger reads the signal from the
 thermocouples and sends this information to a computer with software to display and record the temperature data.

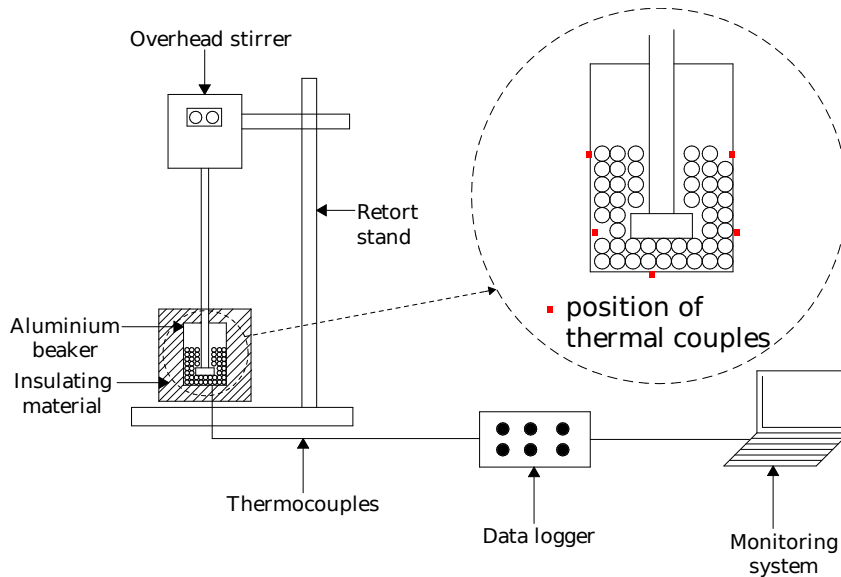


Figure 1: Schematic representation of the experimental setup

102

103 2.2. Experimental procedure, data acquisition and data processing

104 Particle agitation and data recording are started simultaneously and left to run for 4 hours while the temperature of
 105 the beaker is continuously monitored and recorded at each second. The experiment is repeated at least twice to ensure
 106 repeatability. It is assumed that the temperature changes experienced by the aluminium beaker result solely from the
 107 heat generated during the agitation of the particles. Moreover, it is assumed that, after sufficient time, the granular
 108 medium attains a uniform temperature equal to that of the aluminium beaker.

109 To examine the influence of physical properties, spherical particles of lead, steel and glass (see Table 1) are used.
 110 Also, the influence of rotational speed was investigated using blade speeds from 50 to 250 rpm. Additionally, three
 111 particle sizes are investigated where the particle sizes vary between 2.15 – 2.31, 4.01 – 4.15 and 6.33 – 6.34 mm.
 112 Therefore, it can be assumed that each portion had a mono-size distribution of approximate diameter of 2, 4 and 6 mm,
 113 hence the labels ϕ_2 , ϕ_4 and ϕ_6 , respectively. For investigating the effect of fill ratios, four ratios of 25%, 28%, 40%
 114 and 52% are used. The fill ratios are determined by measuring the ratio of the height of the granular bed to that of the
 115 beaker. Furthermore, to explore the impact of blade configurations, blades with dimensions $72 \times 36 \times 2$ mm for length,
 116 width and thickness, respectively, are 3D-printed into three shapes: a curved shape (Type 1), a flat rectangular shape
 117 (Type 2) and a 45° tilted shape (Type 3). Finally, a smaller size (dimensions $60 \times 30 \times 2$ mm) of the curved blade (Type
 118 1*) is used to examine the influence of blade size (See Fig. 2). Table 2 summarises the base conditions for each case
 119 examined.

120 For post processing, data from the five thermocouples are averaged to provide the mean temperature. It is assumed
 121 that this temperature is equivalent to the average temperature of the granular medium. Moreover, the standard deviation
 122 from the five thermocouples provides a region of confidence for the continuous temperature curves. The temperature

Table 1
Material properties of particles used in the experiments.

Material	<i>Glass</i> ^[44]	<i>Steel</i> ^[45]	<i>Lead</i> ^[46]
Young's modulus [GPa]	63.0	200.0	14.0
Density [kg/m ³]	2500	7750	11350
Specific heat capacity [J/kg.K]	1329	460	129
Thermal conductivity [W/m.K]	1.13	24.90	33.00

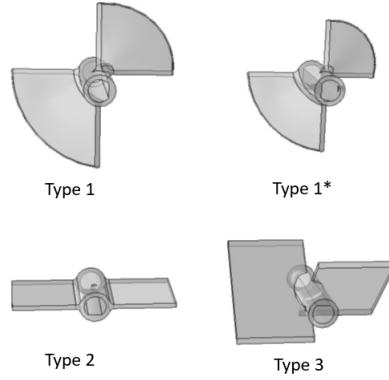


Figure 2: Impeller blades used in the experiments

Table 2
Experimental configurations highlighting the investigated parameters

Case No	Investigated parameter	Material	Particle diameter, ϕ (mm)	Fill ratio (%)	Impeller type	Rotational speed, ω (rpm)
1	Material	Glass, Steel, Lead	ϕ_2 (2.15 – 2.31)	40	Type 1	150
2	Rotational speed	Glass, Steel	ϕ_2 (2.15 – 2.31)	40	Type 1	50-250
3	Fill ratio	Steel	ϕ_2 (2.15 – 2.31)	25, 28, 40, 52	Type 1	150
4	Particle size	Glass, Steel	ϕ_2 ((2.15 – 2.31), ϕ_4 (4.01 – 4.15), ϕ_6 (6.33 – 6.34)	40	Type 1*	150
5	Blade type	Steel	ϕ_2 (2.15 – 2.31)	40	Type 1, Type 2, Type 3	150
6	Blade size	Steel	ϕ_2 (2.15 – 2.31)	40	Type 1, Type 1*	150

123 rise, ΔT , is obtained by subtracting the initial temperature from the average temperature at each time instant. The initial
124 temperature is the room temperature in the laboratory, which was approximately constant (19 – 21°C).

125 It should be noted that, although examining the flow patterns is not a primary focus of the present work, a general
126 overview of the particle dynamics for the current setup is necessary. The aluminium beaker is hence replaced with
127 an acrylic plastic beaker to allow visibility of the particles during the stirring process. It is assumed that the particle
128 dynamics inside the aluminium and acrylic beakers are similar. High-resolution short videos (1080 pixels and 30 Hz)
129 are recorded for all cases presented in Table 2.

130 3. Results and discussion

131 3.1. Flow behaviour

132 Eq (1), is used to estimate the Inertia number, I_0 where the shear rate, γ (s^{-1}) is computed from the rotational
 133 speed, ω (in *rpm*) as [8],

$$\gamma = 2\pi\omega \times \frac{1}{60}(\text{min/s}) \quad (2)$$

134 assuming a hydro-static pressure, the pressure, P on the blade can be calculated as,

$$P = \rho gh \quad (3)$$

135 where g is the gravitational acceleration, and h is the bed height above the blade obtained through image analysis
 136 from the recorded videos, the inertial number, I_0 can be calculated. The results show that at varying rotational speeds
 137 (Case No. 2, Table 2), I_0 lies between 0.04 – 0.19, and at varying particle diameters (Case No. 4, Table 2), I_0 lies
 138 between 0.15 – 0.43. This implies that, except for the slower rotational speed, i.e., 50 *rpm*, the particle flow behaviour
 139 for all configurations tested is predominantly in a rapid regime.

140 The visual observation from the recorded videos (Fig. 3) shows different features depending on the experimental
 141 configuration. Generally, the velocity of particles appears to be higher at the free surface and lower at the bottom of
 142 the bed (see supplementary material). In addition, the free surface forms heaps directly above the blade and troughs in
 143 between. The frequency and the height of the periodic heap-trough shape increase with the rotational speed. Moreover,
 144 at higher speeds, the bed shows a fluid-like behaviour where the height rises, forming a bowl-shaped free surface (Fig.
 145 3a). The bowl-shaped surface is also observed at higher fill ratios (Fig. 3b). When considering different blade types
 146 (Case No. 5 Table 2), the trough is particularly low for blade 2 (Fig. 3c). Moreover, when a smaller-sized blade is used
 147 (Case No. 6, Table 2), the granular bed shows a completely static layer at the bottom of the beaker. When varying the
 148 particle size using a smaller-sized blade (Case No. 4, Table 2), the static bottom layer present for smaller particles (ϕ_2)
 149 is not observed for larger particle sizes, i.e., ϕ_4 and ϕ_6 (Fig. 3d).

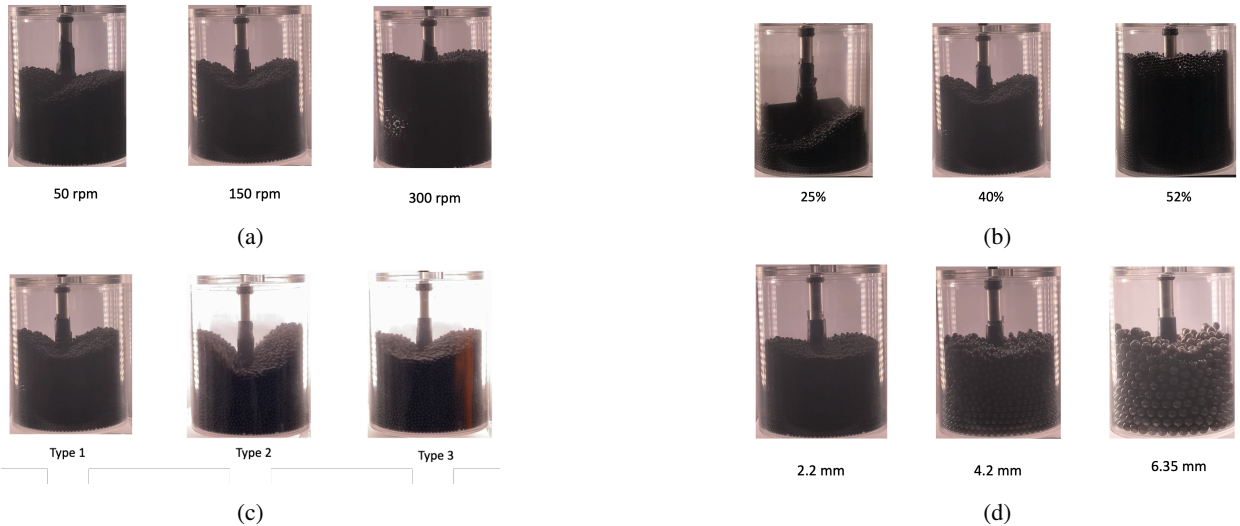
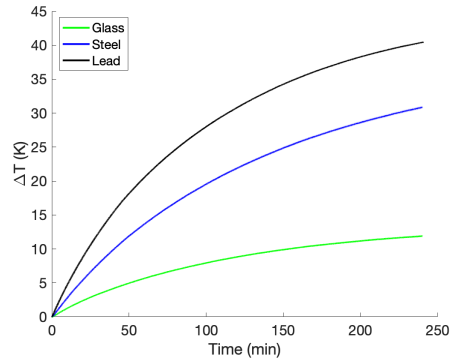


Figure 3: Flow behaviour for different cases with varying (a) rotational speed, (b) fill ratio, (c) blade type and (d) particle size

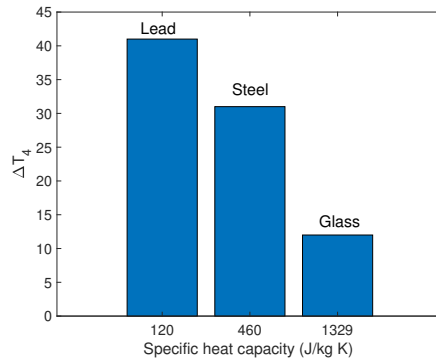
150 3.2. Influence of material type

151 Industrial applications involve a wide range of materials which respond differently to thermo-mechanical loading
 152 depending on their physical properties. In the present study, glass, steel and lead particles were used to investigate

153 the material thermal response to mechanical agitation. Other parameters were kept constant, as presented in Table 2
 154 (Case No. 1). Fig. 4a shows the temperature increase over 4 hours, indicating that lead has the highest temperature
 155 increase, followed by steel, while glass particles show the lowest temperature rise. This behaviour can be attributed to
 156 the physical properties of the materials, mainly density and heat capacity (see Table 1). Lead and steel particles are
 157 denser, implying that at the same agitation speed, they pick up more kinetic energy and thus dissipate more energy
 158 through collisions and friction. Further, owing to their low heat capacity, the metallic particles require less thermal
 159 energy to raise the temperature by the same amount as the other material (glass), which has a relatively higher heat
 160 capacity. This is evident in Fig. 4b where the specific heat capacities are plotted against the maximum temperature
 161 reached at the end of the experiments.



(a)



(b)

Figure 4: (a) Temperature rise evolution for different materials as observed from 4-hour experiments and (b) the maximum attained temperature in function of material's specific heat capacity

162 It can also be observed that temperature curves approach a thermal equilibrium condition where the heat generation
 163 and heat loss rates are equal. However, reaching this thermal equilibrium state requires a longer experimental time.
 164 Therefore, a first-order kinetic equation Eq (4) is used to fit the experimental data and extend it to the equilibrium state.
 165 The fitting parameters are the maximum temperature rise, ΔT_{max} , and the kinetic parameter, k .

$$\frac{\Delta T}{\Delta T_{max}} = 1 - \exp(-kt) \quad (4)$$

166 where ΔT is the current temperature rise and t is the time. Fig. 5 shows the results where the temperature profiles
 167 from Fig. 4a are extended near the equilibrium state using the fitting equation. This procedure is advantageous because
 168 it provides the potential maximum temperature that the granular materials would attain should the experiments run
 169 long enough to reach the thermal equilibrium state. Henceforth, the fitting equation will be used to fit the experimental
 170 results for all cases discussed in this work.

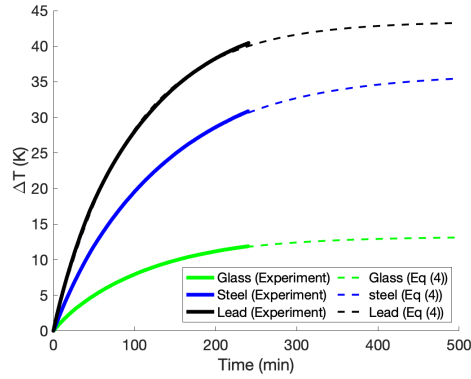


Figure 5: Temperature rise evolution for different materials as observed from 4-hour experiments and extended with the fitting equation (i.e., Eq (4)) to approach the equilibrium state

171 3.3. Influence of rotational speed

172 Blade rotational speed is a key parameter in many applications involving bladed mixers. For example, applications
 173 involving heat and mass transfer rely on optimum agitation speed to maintain a uniform bed temperature. The influence
 174 of the agitation speed was investigated by varying the blade speed between 50 – 250 rpm, as indicated by Case No.
 175 2 in Table 2. The particles are mechanically strong to prevent particle breakage, especially at higher agitation speeds
 176 and no particle breakage and attrition are observed in these experiments.

177 Fig. 6 shows that the temperature rise increases with the rotational speed for both steel and glass particles. It is
 178 clear that the influence of impeller speed is more pronounced for steel where the rate of temperature rise is greater
 179 compared to that of glass particles. This is evident in Fig. 7 where the temperature rise taken at 4 hours (ΔT_4) for all
 180 the rotational speeds is normalised with the temperature rise for the lowest rotational speed (ΔT_{4-50}). For steel particles,
 181 the temperature rise is minimal at the lowest rotational speed (50 rpm) and increases approximately 10 times at the
 182 highest rotational speed (250 rpm). On the other hand, glass particles show lesser values with only 5 times increase
 183 between the rotational speeds of 50 rpm and 250 rpm. Higher blade rotation is associated with higher blade torque and
 184 greater particle kinetic energy. It is evident from the visual observation of particle dynamics where at higher speeds,
 185 the flow is more fluid-like with higher bed height (see Fig. 3a). This implies that particles are pushed more towards the
 186 container wall, increasing the particle-wall friction. Consequently, higher heat generation from both friction and which
 187 leads to a greater temperature increase. The higher rate of temperature rise for steel can be attributed to its physical
 188 properties, notably higher density and low specific heat capacity, which enables the material to generate more heat and
 189 raise the temperature more quickly.

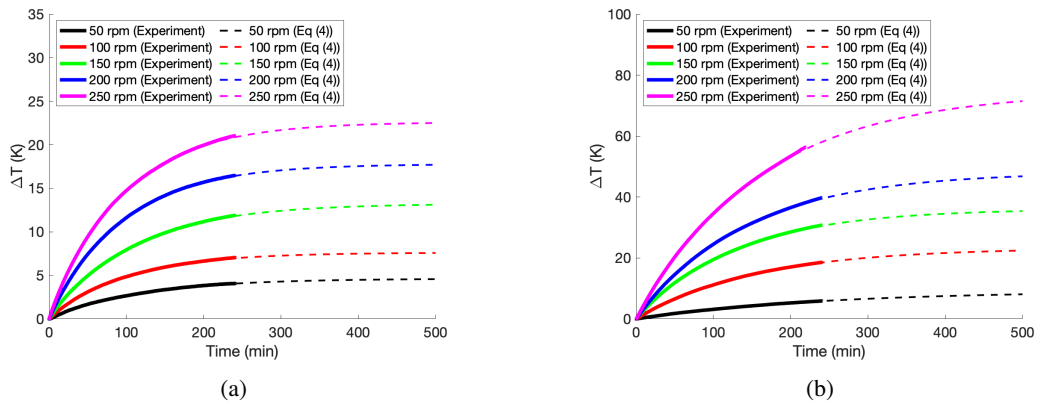


Figure 6: Temperature rise evolution for various rotational speeds as observed from experiments and extended to approaching the equilibrium state by first-order kinetic equation (i.e., Eq (4)): (a) glass and (b) steel particles.

Experimental investigation of heat generation during granular mixing

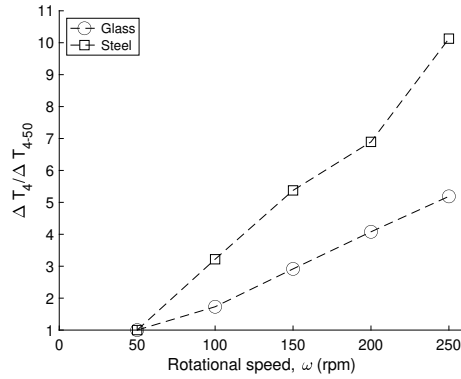


Figure 7: The temperature rise at 4 hours (ΔT_4) with the temperature rise at 4 hours for the 50 rpm (ΔT_{4-50}) and plotted in function of rotational speeds

190 It is worth examining whether the temperature rise is uniquely dictated by the heat dissipation rate (rotational speed)
 191 or net dissipated heat (number of blade revolutions). In Fig. 8, the maximum temperature for equal blade revolutions
 192 is plotted against the rotational speeds. It is observed that the temperature rise is more significant for higher agitation
 193 speed. This is particularly evident for greater blade revolutions where the bed is agitated long enough to achieve higher
 194 temperatures. It implies that the thermal response depends primarily on the blade's rotational speed (heat rate) rather
 195 than the number of the blade passes (net heat). At lower blade revolutions, the bed temperature appears to be less
 196 different, which may suggest that the net heat is the main driving aspect of temperature. However, it can also be due
 197 to the low temperatures at the initial stages of bed agitation; hence the difference in temperature rise for different
 198 rotational speeds is not yet vivid.

199 This observation is attributed to the readiness of the system to approach thermal equilibrium. When stirred at
 200 lower speeds, the granular bed takes longer to generate the same amount of heat than agitations at higher speeds. For
 201 example, 8000 blade revolutions correspond to 32 and 160 minutes of running time for the agitation speeds of 250 rpm
 202 and 50 rpm, respectively. Consequently, in low-speed cases, the temperature rise is limited because the slower rate of
 203 heat generation provides sufficient time for heat loss to the surroundings, thus readily approaching thermal equilibrium.
 204 It should also be noted that a change in the flow regime would be expected to change the heat dissipation rate.

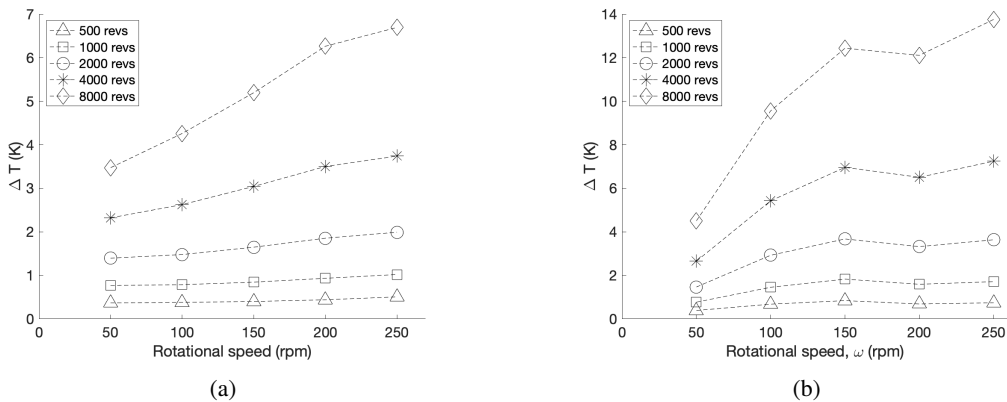


Figure 8: The temperature rise in function of rotational speeds for a specific number of blade revolutions: (a) glass and (b) steel particles.

3.4. Influence of fill ratio

205 The weight of the granular bed can influence stress distribution and flow dynamics [11]. Therefore, it is vital to
 206 explore its effect on heat generation in this study by examining four fill ratios denoted by Case No. 3 in Table 2. Fig. 9
 207

208 shows the results for varied fill ratios where steel particles are used. Generally, the temperature rise is more significant
 209 as the fill ratio increases. Interestingly, the highest fill ratio (52%) shows a slower trend in temperature rise at the
 210 initial stages. We hypothesise that this is related to the longer time needed for the denser medium to attain a uniform
 temperature.

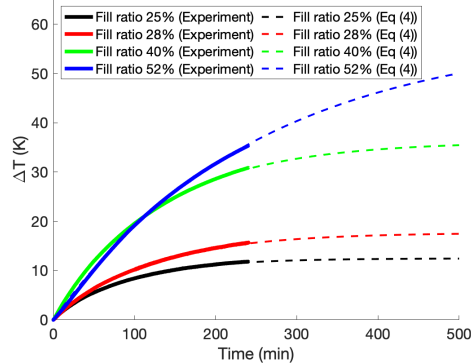


Figure 9: Temperature rise evolution for different fill ratios as observed from experiments and extended to approaching the equilibrium state by first-order kinetic equation.

211
 212 When particles are filled above the blade span, the pressure distribution within the granular medium becomes
 213 approximately hydrostatic [40]. Therefore, at higher fill ratios, greater pressure is acting on the particles from those
 214 above the blade, leading to a greater resistance for the blade to overcome. This was also confirmed by Boonkanokwong
 215 et al [8], who showed that the impeller torque was greater for higher fill ratios. Therefore, more energy is dissipated
 216 to overcome the greater frictional force exerted by a larger fill ratio, resulting in more heat generation and greater
 217 temperature rise. Additionally, as shown in the flow behaviour images (Fig. 3b), the low fill ratios are characterised by
 218 the heap-valley free surface. Such features promote recirculation zones in which the vertical and radial velocities are
 219 predominant [11] thus limiting the frictional work by tangential velocity. In contrast, the tangential velocities become
 220 more dominant for higher fill ratios (marked by the bowl-shaped free surface), resulting in more frictional heat from
 221 the particle-wall contact.

222 3.5. Influence of particle size

223 It is essential to investigate the influence of particle size due to its central role in granular flow regimes and scale-up
 224 applications [11]. Three particle diameters were selected from steel and glass as described by Case No. 4 in Table 1.
 225 The fill ratio was kept constant by maintaining the total mass of each portion. A smaller-sized blade was used to ensure
 226 a smooth agitation, especially of the large-sized particles. It is observed in Fig. 10 that, generally, the temperature
 227 rise increases with the particle size. This is especially true for glass beads. For steel particles, the temperature rise
 228 increases between ϕ_2 and ϕ_4 . However, the temperature rise decreases from ϕ_4 to ϕ_6 , such that the smallest and
 229 largest diameters of steel particles provide approximately the same curve for temperature rise. It is worth pointing
 230 out that the lesser temperature rise for the ϕ_6 steel particles could result from their different surface characteristics.
 231 It was noticed that these particles (coming from a different supplier) had a polished surface, implying that they had
 232 a lower friction coefficient, which leads to reduced friction-induced heat. Also, it was observed that the larger steel
 233 particles can get stuck within the bottom or lateral clearance and block the blade from rotating continuously. This leads
 234 to temperature noises evident in Fig. 10b.

235 As particle size increases, the frictional force between each particle is enhanced, increasing the resistance the blade
 236 must overcome to agitate the medium. This was evident in the particle dynamics (Fig. 3d) where it was observed that for
 237 smaller-size particles the bottom layer was stagnant, while for large particles the whole bed was agitated. Consequently,
 238 more energy is dissipated, resulting in more heat generation. This was also confirmed by Boonkanokwong et al. [8],
 239 who reported that the blade torque and system power consumption were more significant for larger particles.

240 3.6. Influence of blade shape

241 Blade configuration plays a crucial role in dictating particle movement and mixer performance. Therefore, three
 242 blade shapes (Type 1, Type 2 and Type 3 in Fig. 2) having equal surface area are selected to investigate the influence of

Experimental investigation of heat generation during granular mixing

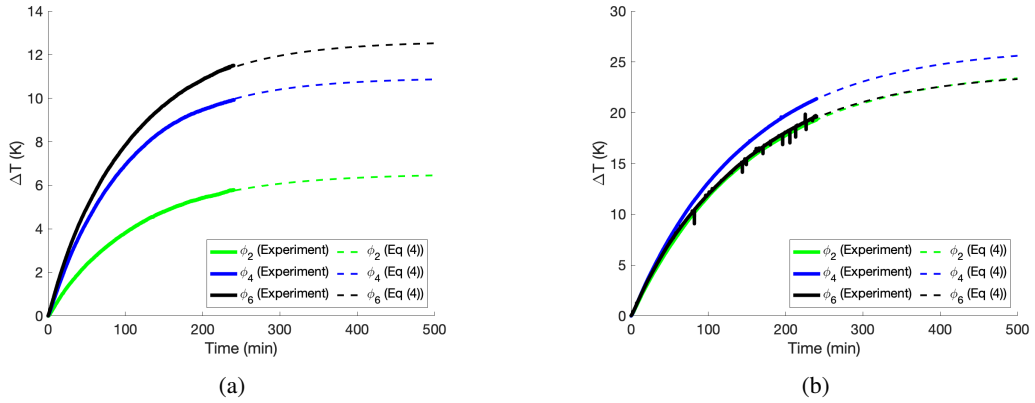


Figure 10: Temperature rise evolution for different particle sizes as observed from experiments and extended to approaching the equilibrium state by first-order kinetic equation (i.e., Eq (4)): (a) glass and (b) steel particles.

243 blade shape. Other parameters remained constant as described by Case No. 5 in Table 2. The results in Fig. 11 suggest
 244 that the granular medium experiences the highest temperature rise when a flat rectangular blade (Type 2) is used for
 245 agitation. However, the temperature rise over four hours is about 35% lower when the tilted blade (Type 3) is used. For
 246 the curved blade (Type 1), the bed experiences a temperature rise at values lying between the two extremes. As evident
 247 from the particle flow behaviour, the granular medium agitated by the Type 2 blade shows a remarkably steep trough
 248 (Fig. 3c) indicating that more particles are pushed towards the container wall. Therefore the rectangular blade (Type
 249 2) imparts a more tangential flow leading to great frictional energy dissipation between the particles and the container
 250 wall. Consequently, more heat is generated leading to greater temperature rise. It was also confirmed by others [7, 8]
 251 that the torque exerted on the granular medium is highest for the blade tilt of 90° (rectangular blade) and decreases
 with the tilt angle.

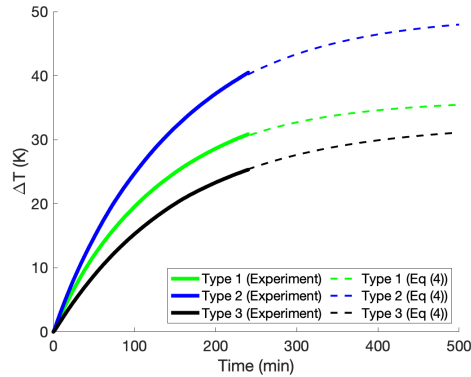


Figure 11: Temperature rise evolution for different blade types as observed from experiments and extended to approaching the equilibrium state by first-order kinetic equation (i.e., Eq (4)).

252

253 3.7. Influence of blade size

254 The influence of blade size was also examined, where blades Type 1 and Type 1* (see Fig. 2) were selected as
 255 indicated by Case No. 6 in Table 2. Fig. 12 reveals that the granular medium experiences a higher temperature rise
 256 when a larger blade is used. The particles in front of the blade resist the blade motion at a rate proportional to the blade
 257 area [11]. Therefore, the blades with larger sizes exert more torque due to the particles' greater resistance as more of
 258 the bed is mobilised, leading to more heat generation and a greater temperature increase. Additionally, the presence of
 259 a stagnant layer at the bottom of the beaker suggests that fewer particles are being agitated hence less heat generation.

260 This observation is also confirmed by Boonkanokwong et al. [8], where larger torques were recorded for larger blades
 261 and vice versa.

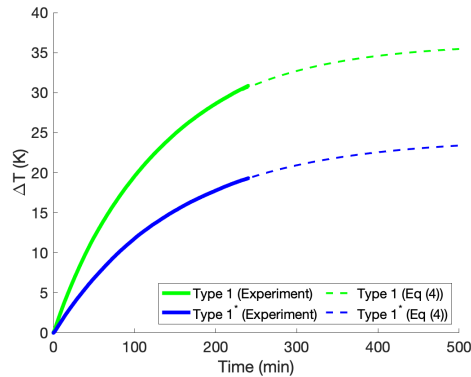


Figure 12: Temperature rise evolution for different blade sizes as observed from experiments and extended to approaching the equilibrium state by first-order kinetic equation (i.e., Eq (4)).

262 4. Data Availability and Reproducibility Statement

263 The numerical experimental data for Figs. 5-12 related to Case No. 1-6 are included as 'RawData.zip' in the
 264 supplementary materials for each case number, as highlighted in Table. 2. The fitting parameters used in Eq (4) for
 265 Cases No. 1-6 are also given in the appendix. The video data for particle dynamics for representative cases No. 2 and 6
 266 are also added as supplementary material as 'Video_Data.zip'. The two cases are selected to demonstrate the particle
 267 motion that appears to be slow at the bottom and faster at the top of the container. Such information could not be
 268 captured in the images in Fig. 3.

269 5. Conclusions

270 For the wide range of parameters investigated, it was demonstrated that metallic particles (lead and steel) are
 271 susceptible to more heat generation due to their high density and low specific heat capacity which cause them to heat
 272 up faster than the non-metallic particles (glass). It was also observed that at lower blade revolutions, the temperature rise
 273 is lesser and therefore hardly distinguishable for all blade rotational speeds. However, the trend changes for increased
 274 blade revolutions where the temperature increase is more significant for higher rotational speeds, indicating that rotation
 275 speed (heat rate) plays a vital role in the thermal response of the granular bed. This information is vital for applications
 276 such as drying, where a debate of optimum agitation speed for an efficient drying process is still open. A higher fill
 277 ratio causes greater pressure on the particles along and below the blade, leading to greater resistance for the blade to
 278 overcome. Consequently, more heat is generated and a greater temperature rise in the bed. However, it was observed
 279 that the initial rate of increase of temperature is low for higher fill ratios due to the longer time needed to heat the large
 280 volume of granular medium. Additionally, for larger particles, the whole bed is agitated, leading to a faster and greater
 281 temperature rise. The blade shape also plays a significant role in the granular flow. For example, tilting the blade to
 282 45° reduces the maximum temperature rise by more than 35 % compared to a vertical blade of the same area.

283 The present study offers insightful results on the thermal response of granular media. The temperature rise
 284 corresponds to the generated heat, which is related to the amount of power consumed and subsequently dissipated
 285 by the granular medium during agitation. Others also showed such observations [7, 8, 40], confirming that the torque
 286 exerted by the blades to the granular medium increases with blade size, fill ratio, rotating speed and particle size.
 287 However, further investigation is required to better understand the heat generation behaviour of granular materials,
 288 particularly in quantifying the generated heat and other forms of energy. In the subsequent studies, we aim to explore
 289 these issues by measuring experimentally the energy consumed by the system and investigating how that energy is
 290 transformed into other forms of energy such as kinetic and thermal energy. Furthermore, the experimental results
 291 presented in this work can be instrumental in validating and calibrating numerical simulations.

Acknowledgements

This project is funded through Marie SKŁODOWSKA-CURIE Innovative Training Network MATHEGRAM, the People Programme (Marie SKŁODOWSKA-CURIE Actions) of the European Union's Horizon 2020 Programme H2020 under REA grant agreement No. 813202.

References

- [1] R. D. Lorenz, "A theory of angel hair: Analytic prediction of frictional heating of particulates in pneumatic transport," *Powder Technology*, vol. 355, pp. 264–267, 2019.
- [2] A. Michaud, R. Pecszalski, and J. Andrieu, "Experimental study and modeling of crystalline powders vacuum contact drying with intermittent stirring," *Drying Technology*, vol. 25, no. 7-8, pp. 1163–1173, 2007.
- [3] A. Michaud, R. Pecszalski, and J. Andrieu, "Modeling of vacuum contact drying of crystalline powders packed beds," *Chemical Engineering and Processing: Process Intensification*, vol. 47, no. 4, pp. 722–730, 2008.
- [4] C. D. Papageorgiou, M. Langston, F. Hicks, D. am Ende, E. Martin, S. Rothstein, J. Salan, and R. Muir, "Development of screening methodology for the assessment of the agglomeration potential of apis," *Organic Process Research & Development*, vol. 20, no. 8, pp. 1500–1508, 2016.
- [5] A. S. Mujumdar, *Handbook of industrial drying*. CRC press, 2006.
- [6] M. Murru, G. Giorgio, S. Montomoli, F. Ricard, and F. Stepanek, "Model-based scale-up of vacuum contact drying of pharmaceutical compounds," *Chemical Engineering Science*, vol. 66, no. 21, pp. 5045–5054, 2011.
- [7] P. Knight, J. Seville, A. Wellm, and T. Instone, "Prediction of impeller torque in high shear powder mixers," *Chemical Engineering Science*, vol. 56, no. 15, pp. 4457–4471, 2001.
- [8] V. Boonkanokwong, R. P. Frank, P. Valliappan, B. Remy, J. G. Khinast, and B. J. Glasser, "Flow of granular materials in a bladed mixer: effect of particle properties and process parameters on impeller torque and power consumption," *Advanced Powder Technology*, vol. 29, no. 11, pp. 2733–2752, 2018.
- [9] A. Boateng and P. Barr, "Granular flow behaviour in the transverse plane of a partially filled rotating cylinder," *Journal of Fluid Mechanics*, vol. 330, pp. 233–249, 1997.
- [10] A. Sack and T. Pöschel, "Dissipation of energy by dry granular matter in a rotating cylinder," *Scientific Reports*, vol. 6, no. 1, pp. 1–9, 2016.
- [11] B. Remy, W. Kightlinger, E. M. Saurer, N. Domagalski, and B. J. Glasser, "Scale-up of agitated drying: Effect of shear stress and hydrostatic pressure on active pharmaceutical ingredient powder properties," *AIChE Journal*, vol. 61, no. 2, pp. 407–418, 2015.
- [12] E. W. Conder, A. S. Cosbie, J. Gaertner, W. Hicks, S. Huggins, C. S. MacLeod, B. Remy, B.-S. Yang, J. D. Engstrom, D. J. Lamberto, *et al.*, "The pharmaceutical drying unit operation: an industry perspective on advancing the science and development approach for scale-up and technology transfer," *Organic Process Research & Development*, vol. 21, no. 3, pp. 420–429, 2017.
- [13] M. Ebrahimi, E. Siegmann, D. Prieling, B. J. Glasser, and J. G. Khinast, "An investigation of the hydrodynamic similarity of single-spout fluidized beds using cfd-dem simulations," *Advanced Powder Technology*, vol. 28, no. 10, pp. 2465–2481, 2017.
- [14] A. Chaudhury, A. Niziolek, and R. Ramachandran, "Multi-dimensional mechanistic modeling of fluid bed granulation processes: an integrated approach," *Advanced Powder Technology*, vol. 24, no. 1, pp. 113–131, 2013.
- [15] Y. Sato, H. Nakamura, and S. Watano, "Numerical analysis of agitation torque and particle motion in a high shear mixer," *Powder Technology*, vol. 186, no. 2, pp. 130–136, 2008.
- [16] R. Stewart, J. Bridgwater, Y. Zhou, and A. Yu, "Simulated and measured flow of granules in a bladed mixer—a detailed comparison," *Chemical Engineering Science*, vol. 56, no. 19, pp. 5457–5471, 2001.
- [17] Y. Zhou, A. Yu, and J. Bridgwater, "The effect of blade speed on granular flow in a cylindrical mixer," in *Proceedings of World Congress on Particle Technology*, vol. 4, pp. 21–25, 2002.
- [18] C. Hartmanshenn, P. Chaksmithanont, C. Leung, D. V. Ghare, N. Chakraborty, S. Patel, M. Halota, J. G. Khinast, C. D. Papageorgiou, C. Mitchell, *et al.*, "Infrared temperature measurements and dem simulations of heat transfer in a bladed mixer," *AIChE Journal*, p. e17636, 2022.
- [19] G. M. gdrmidi@ polytech. univ-mrs. fr <http://www.lmgc.univ-montp2.fr/MIDI/>, "On dense granular flows," *The European Physical Journal E*, vol. 14, pp. 341–365, 2004.
- [20] F. Radjai and F. Dubois, "Discrete numerical modeling of granular materials, vol. isbn: 978-1-84821-260-2," 2011.
- [21] G. Combe and J.-N. Roux, "Discrete numerical simulation, quasistatic deformation and the origins of strain in granular materials," *arXiv preprint arXiv:0901.3842*, 2009.
- [22] S. Savage, "Analyses of slow high-concentration flows of granular materials," *Journal of Fluid Mechanics*, vol. 377, pp. 1–26, 1998.
- [23] B. Miller, C. O'Hern, and R. Behringer, "Stress fluctuations for continuously sheared granular materials," *Physical Review Letters*, vol. 77, no. 15, p. 3110, 1996.
- [24] M. A. Hopkins and M. Y. Louge, "Inelastic microstructure in rapid granular flows of smooth disks," *Physics of Fluids A: Fluid Dynamics*, vol. 3, no. 1, pp. 47–57, 1991.
- [25] G. I. Tardos, S. McNamara, and I. Talu, "Slow and intermediate flow of a frictional bulk powder in the couette geometry," *Powder Technology*, vol. 131, no. 1, pp. 23–39, 2003.
- [26] J. McCarthy, T. Shinbrot, G. Metcalfe, J. E. Wolf, and J. M. Ottino, "Mixing of granular materials in slowly rotated containers," *AIChE Journal*, vol. 42, no. 12, pp. 3351–3363, 1996.
- [27] K. Malhotra and A. Mujumdar, "Particle mixing and solids flowability in granular beds stirred by paddle-type blades," *Powder Technology*, vol. 61, no. 2, pp. 155–164, 1990.

351 [28] Y. Saito, A. Ingram, X. Fan, and J. P. K. Seville, "Effects of blade design in wet granulation in a high shear mixer determined by positron
352 emission particle tracking," *Journal of Environment and Engineering*, vol. 6, no. 1, pp. 233–241, 2011.

353 [29] Y. Saito, X. Fan, A. Ingram, and J. P. K. Seville, "Pept analysis of impeller blade geometry and averaged velocity in a high shear mixer,"
354 *Journal of Fluid Science and Technology*, vol. 6, no. 2, pp. 169–176, 2011.

355 [30] J. Doucet, F. Bertrand, and J. Chaouki, "An extended radioactive particle tracking method for systems with irregular moving boundaries,"
356 *Powder Technology*, vol. 181, no. 2, pp. 195–204, 2008.

357 [31] I. Govender, A. McBride, and M. Powell, "Improved experimental tracking techniques for validating discrete element method simulations of
358 tumbling mills," *Experimental Mechanics*, vol. 44, no. 6, pp. 593–607, 2004.

359 [32] T. A. Kingston, T. A. Geick, T. R. Robinson, and T. J. Heindel, "Characterizing 3d granular flow structures in a double screw mixer using
360 x-ray particle tracking velocimetry," *Powder Technology*, vol. 278, pp. 211–222, 2015.

361 [33] H. Nadeem and T. J. Heindel, "Review of noninvasive methods to characterize granular mixing," *Powder Technology*, vol. 332, pp. 331–350,
362 2018.

363 [34] M. Sinnott and P. Cleary, "3d dem simulations of a high shear mixer," in *Third International Conference on CFD in the minerals and Process
364 Industries CSIRO, Melbourne, Australia*, 2003.

365 [35] Y. C. Zhou, A. B. Yu, and J. Bridgwater, "Segregation of binary mixture of particles in a bladed mixer," *Journal of Chemical Technology &
366 Biotechnology: International Research in Process, Environmental & Clean Technology*, vol. 78, no. 2-3, pp. 187–193, 2003.

367 [36] Y. Zhou, A. Yu, R. Stewart, and J. Bridgwater, "Microdynamic analysis of the particle flow in a cylindrical bladed mixer," *Chemical
368 Engineering Science*, vol. 59, no. 6, pp. 1343–1364, 2004.

369 [37] T. Barczy, T. Travnickova, J. Havlica, and M. Kohout, "Effect of bed depth on granular flow and homogenization in a vertical bladed mixer via
370 discrete element method," *Chemical Engineering & Technology*, vol. 38, no. 7, pp. 1195–1202, 2015.

371 [38] Z. Zuo, S. Gong, and G. Xie, "Numerical investigation of granular mixing in an intensive mixer: Effect of process and structural parameters
372 on mixing performance and power consumption," *Chinese Journal of Chemical Engineering*, vol. 32, pp. 241–252, 2021.

373 [39] I. Gijón-Arreortúa and A. Tecante, "Mixing time and power consumption during blending of cohesive food powders with a horizontal helical
374 double-ribbon impeller," *Journal of Food Engineering*, vol. 149, pp. 144–152, 2015.

375 [40] Y. Bao, J. Liu, H. Yang, Z. Cai, and Z. Gao, "Shaft power consumption of stirred tank with particles: From the perspective of pseudoshearing
376 thinning rheological property of particles," *Industrial & Engineering Chemistry Research*, 2022.

377 [41] D. H. Wagner, S. Ramanathan, M. L. Taylor, A. B. Brown, M. E. S. Wobker, and M. W. Prior, "The thermodynamics of high shear blending,"
378 *Powder Technology*, vol. 193, no. 2, pp. 195–199, 2009.

379 [42] Z. Sun, H. Zhu, and J. Hua, "Granular flow characteristics and heat generation mechanisms in an agitating drum with sphere particles:
380 Numerical modeling and experiments," *Powder Technology*, vol. 339, pp. 149–166, 2018.

381 [43] E. K. Sahni, R. H. Bogner, and B. Chaudhuri, "Systematic investigation of parameters affecting the performance of an agitated filter-dryer,"
382 *Journal of Pharmaceutical Sciences*, vol. 102, no. 7, pp. 2198–2213, 2013.

383 [44] https://www.sigmund-lindner.com/wp-content/uploads/2018/08/SiLibeads_Type_S-1.pdf. (Accessed: 2022-09-01).

384 [45] [https://www.pennstainless.com/resources/product-information/stainless-grades/400-series/
385 420-stainless-steel](https://www.pennstainless.com/resources/product-information/stainless-grades/400-series/420-stainless-steel). (Accessed: 2022-09-01).

386 [46] <https://www.matweb.com/search/DataSheet.aspx?MatGUID=ebd6d2cdfdca4fc285885cc4749c36b1>. (Accessed: 2022-09-01).

387 Appendix

388 The first-order kinetic equation is used to fit the experimental data and extend the results beyond the experimental
389 time (4 hours). For each case, two fitting parameters are used, namely the maximum temperature ΔT_{max} and a kinetic
390 parameter k which is the reciprocal of the time used for the bed to reach about 60% of the maximum temperature. In
391 the tables, the values of fitting parameters for all the cases discussed in this work are summarised.

Table 3
Case No. 1: varying materials, data presented in Fig. 5

Material	ΔT_{max} (K)	k^{-1} (min)	R^2	RSME
Glass	13.25	108.2	0.9996	0.0615
Steel	36.19	128	0.9998	0.1206
Lead	95.23	95.25	0.9993	0.2978

Table 4

Case No. 2: varying blade rotational speed - Glass, data presented in Fig. 6a

Rotational speed (<i>rpm</i>)	ΔT_{max} (K)	k^{-1} (min)	R^2	RSME
50	4.6	114.9	0.9994	0.0284
100	7.624	97.61	0.9996	0.0380
150	13.25	108.2	0.9996	0.0615
200	17.79	93.71	0.9999	0.0454
250	22.62	94	0.9996	0.1147

Table 5

Case No. 2: varying blade rotational speed - Steel, data presented in Fig. 6b

Rotational speed (<i>rpm</i>)	ΔT_{max} (K)	k^{-1} (min)	R^2	RSME
50	9.2	236.2	0.9998	0.0217
100	23.34	152.3	1	0.0367
150	36.13	128.4	0.9998	0.1167
200	48.19	140.7	0.9999	0.1225
250	74.82	160.7	0.9998	0.2092

Table 6

Case No. 3: varying container fill ratio, data presented in Fig. 9

Fill ratio (%)	ΔT_{max} (K)	k^{-1} (min)	R^2	RSME
25	12.48	87.35	0.9990	0.0992
28	17.7	115.1	0.9995	0.0916
40	36.19	128	0.9998	0.1206
52	58.14	253	0.9995	0.2382

Table 7

Case No. 4: varying particle size for glass, data presented in Fig.10a

Diameter	ΔT_{max} (K)	k^{-1} (min)	R^2	RSME
ϕ_2	6.54	113.2	0.9999	0.0187
ϕ_4	10.94	99.36	0.9999	0.0283
ϕ_6	12.62	101.9	0.9997	0.0544

Table 8

Case No. 4: varying particle size for steel, data presented in Fig. 10b

Diameter	ΔT_{max} (K)	k^{-1} (min)	R^2	RSME
ϕ_2	24.3	151.7	1	0.0349
ϕ_4	26.48	146.4	1	0.0380
ϕ_6	24.07	144.2	0.9998	0.0814

Table 9

Case No. 5 & No.6: varying blade shape & size, data presented in Figs. 11 and 12

Blade shape/size	ΔT_{max} (K)	k^{-1} (min)	R^2	RSME
Type 1*	24.3	151.7	1	0.0349
Type 1	36.19	128	0.9998	0.1206
Type 2	49.52	143.9	0.9999	0.1294
Type 3	32.49	157.9	0.9999	0.0560